



**HAL**  
open science

## High Frequency Acoustic On-Chip Integration for Particle Characterization and Manipulation in Microfluidics

Sizhe Li, Julien Carlier, Malika Toubal, Huiqin Liu, Pierre Campistron, Dorothee Callens, Georges Nassar, Bertrand Nongaillard, Shishang Guo

► **To cite this version:**

Sizhe Li, Julien Carlier, Malika Toubal, Huiqin Liu, Pierre Campistron, et al.. High Frequency Acoustic On-Chip Integration for Particle Characterization and Manipulation in Microfluidics. *Applied Physics Letters*, 2017, 111 (16), pp.163503. 10.1063/1.5003414 . hal-03258701

**HAL Id: hal-03258701**

**<https://hal.science/hal-03258701>**

Submitted on 27 May 2022

**HAL** is a multi-disciplinary open access archive for the deposit and dissemination of scientific research documents, whether they are published or not. The documents may come from teaching and research institutions in France or abroad, or from public or private research centers.

L'archive ouverte pluridisciplinaire **HAL**, est destinée au dépôt et à la diffusion de documents scientifiques de niveau recherche, publiés ou non, émanant des établissements d'enseignement et de recherche français ou étrangers, des laboratoires publics ou privés.

# High frequency acoustic on-chip integration for particle characterization and manipulation in microfluidics

Cite as: Appl. Phys. Lett. **111**, 163503 (2017); <https://doi.org/10.1063/1.5003414>

Submitted: 05 September 2017 • Accepted: 05 October 2017 • Published Online: 17 October 2017

Sizhe Li, Julien Carlier, Malika Toubal, et al.

## COLLECTIONS

Paper published as part of the special topic on [Acoustic Tweezers](#)



View Online



Export Citation



CrossMark

## ARTICLES YOU MAY BE INTERESTED IN

[Three-dimensional ultrasonic trapping of micro-particles in water with a simple and compact two-element transducer](#)

Applied Physics Letters **111**, 094101 (2017); <https://doi.org/10.1063/1.4992092>

[Acoustic tweezers and motor for living cells](#)

Applied Physics Letters **116**, 123503 (2020); <https://doi.org/10.1063/5.0002327>

[Microbubble enhanced acoustic tweezers for size-independent cell sorting](#)

Applied Physics Letters **116**, 073701 (2020); <https://doi.org/10.1063/1.5123544>

Lock-in Amplifiers  
up to 600 MHz



Zurich  
Instruments



## High frequency acoustic on-chip integration for particle characterization and manipulation in microfluidics

Sizhe Li,<sup>1,2</sup> Julien Carlier,<sup>2,a)</sup> Malika Toubal,<sup>2</sup> Huiqin Liu,<sup>1</sup> Pierre Campistron,<sup>2</sup> Dorothee Callens,<sup>2</sup> Georges Nassar,<sup>2</sup> Bertrand Nongaillard,<sup>2</sup> and Shishang Guo<sup>1,b)</sup>

<sup>1</sup>Key Laboratory of Artificial Micro- and Nano-structures of Ministry of Education, School of Physics and Technology, Wuhan University, Wuhan 430072, China

<sup>2</sup>University of Valenciennes, CNRS, University of Lille, YNCREA, Centrale Lille, UMR 8520 - IEMN, DOAE, F-59313 Valenciennes, France

(Received 5 September 2017; accepted 5 October 2017; published online 17 October 2017)

This letter presents a microfluidic device that integrates high frequency (650 MHz) bulk acoustic waves for the realization of particle handling on-chip. The core structure of the microfluidic chip is made up of a confocal lens, a vertical reflection wall, and a ZnO film transducer coupled with a silicon substrate for exciting acoustic beams. The excited acoustic waves propagate in bulk silicon and are then guided by a 45° silicon mirror into the suspensions in the microchannel; afterwards, the acoustic energy is focused on particles by the confocal lens and reflected by a reflection wall. Parts of the reflected acoustic energy backtrack into the transducer, and acoustic attenuation measurements are characterized for particle detection. Meanwhile, a strong acoustic streaming phenomenon can be seen around the reflection wall, which is used to implement particle manipulation. This platform opens a frontier for on-chip integration of high sensitivity acoustic characterization and localized acoustic manipulation in microfluidics. *Published by AIP Publishing.*

<https://doi.org/10.1063/1.5003414>

Commercialized acoustic sensors in medicine have made great progress in the past few decades. The representative ultrasound probe based devices are ultrasonography,<sup>1</sup> d-mode ultrasonic diagnostic apparatus,<sup>2</sup> and scanning acoustic microscopy.<sup>3</sup> Otherwise, ultrasonic methods are particularly applicable to cell tests and medical diagnosis, because the acoustic technique can implement a gentle way to biological samples in a non-contact mode and characterize their stiffness. Benefiting from this characteristic, scientists integrate acoustic modulus into microelectromechanical system (MEMS) devices for faster cost effectiveness, response time, and mass production capability. In recent years, microfluidics platform has a booming development in clinical diagnosis and new drug screening, due to the unique advantages of fast-response, real time, high sensitivity, and low cost detection and analysis.<sup>4</sup> The acoustic-microfluidic chip technique is developed for on-chip specimen detection and manipulation, which combines both the advantages of ultrasonic technology and miniaturized platform. The highly integrated platform shows great abilities for precise manipulation of tiny samples in biology (proteins, cells, and micro-organisms on the micrometer scale) and *in-situ* detection analysis.

Currently, the acoustic-microfluidics applications are mainly two parts: acoustic sensors for signal processing and acoustic actuators for sample preparation. The acoustic bio-sensing applications concerned with quartz crystal microbalance (QCM) sensors<sup>5</sup> and surface acoustic wave (SAW) based sensors.<sup>6</sup> These types of acoustic detectors require no-labeling of buffer media and avoid photo-bleaching.<sup>7</sup> However, the test sample has to be coupled on the surface of

the oscillating crystal, and the detection distance is limited to the close vicinity of the sensor surface. Then, the flexibility of the active area and sample concentration are restricted. On the other hand, the acoustic actuators are implemented for fast actuation of fluids<sup>8</sup> and efficient manipulation of objects on the micro/nano-scale (particles, cells, and organisms).<sup>9</sup> So far, the principal means for the on-chip actuator modulus concludes: bulk standing acoustic wave (BSAW),<sup>10,11</sup> surface standing acoustic wave (SSAW),<sup>12,13</sup> and traveling surface acoustic wave (TSAW) induced acoustic streaming.<sup>14–16</sup> The standing wave methods critically depend on the compressibility contrast and size of samples, so the sub-micron particle manipulation lacks high sensitivity on account of the limitation of the channel width and acoustic wavelength, while the surface acoustic streaming technique can actuate objects independent of these properties. Therefore, this technique is potentially suitable for driving sub-micron particles, for instance, microvesicles, bacteria, and virus. But the high frequency surface acoustic device is hard to be fabricated in silicon based substrates, which restricts the cost reduction and high integration. Furthermore, as traditional diagnostic tests are commonly implemented at central laboratories with bench-top analyzers, the acoustic integrated device shows potential for cancer cell detection in the future.<sup>16</sup>

Herein, we introduce a high frequency bulk acoustic modulus (650 MHz) integrated microfluidic chip for acoustic characterization and focused acoustic streaming actuation. The acoustic beams propagate through the silicon substrate and are focused into the microchannel. In the lens microchannel, particles are detected when passing through the focus area. In the T shape focused channel, strong acoustic streaming is performed for particles' fast mixing and screening. Therefore, this work demonstrates a feasible integration

<sup>a)</sup>E-mail: julien.carlier@univ-valenciennes.fr

<sup>b)</sup>E-mail: gssyhx@whu.edu.cn

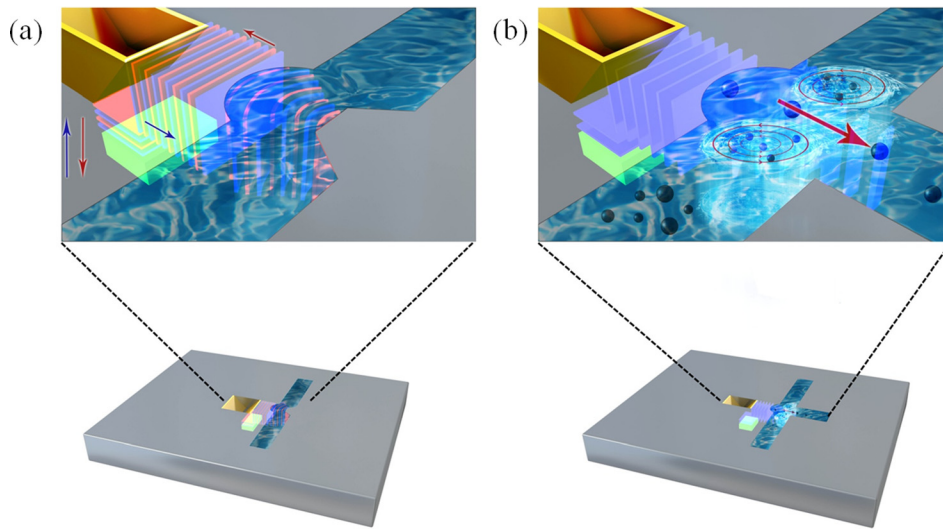


FIG. 1. Schematic diagram of the microsystem for excited acoustic beams propagating in bulk silicon, reflected by the  $45^\circ$  mirror, focused in the confocal lens within the microchannel, and reflected by the reflection wall and then backtrack. (a) Acoustic characterization for particle detection and (b) acoustic manipulation for particle mixing and separation. Blue planes/arrows indicate the transmission paths of the generated acoustic waves, and red planes/arrows indicate the reflection paths of the reflected acoustic waves.

of localized acoustic sensors and actuators in the same microsystem.

For acoustic detection, a reflection mode is designed with a reflection plane placed in the focused plane of the lens, as shown in Fig. 1(a). The acoustic platform is made up of five parts: (1) a  $45^\circ$  silicon mirror plane structure for acoustic wave guiding; (2) a gold film as a matching layer deposited on the  $45^\circ$  mirror; (3) a microchannel with a cylindrical structure for particle detection and actuation; (4) a ZnO film used as a transducer for acoustic beam emitting and receiving; and (5) Polydimethylsiloxane (PDMS) bonding on silicon for device package. The propagated acoustic beams in silicon are reflected by the  $45^\circ$  mirror so that the direction of the beams is parallel to the flat of silicon wafer. Experimental details can be found in our previous work.<sup>17</sup> A gold film is deposited on surfaces of  $45^\circ$  mirrors to avoid mode conversion in acoustic reflection. In our case, a  $1.2\ \mu\text{m}$  thick gold film is matched for 500 MHz central frequency because lower frequency is better for acoustic manipulation due to lower acoustic attenuation and then most longitudinal wave energy can be kept in the wave propagation.<sup>18,19</sup> For acoustic actuation, a T-design is chosen to push the particles in an orthogonal direction, as shown in Fig. 1(b). A 650 MHz frequency is used considering the frequency dependent parameters, which represents the best compromise. When the acoustic beam is focused, the dimensions of the spot in the focal plane are in the range of the wavelength. In this range of frequency, the wavelength in water is of a few microns ( $1.5\ \mu\text{m}$  at 1 GHz). After waveguiding, the acoustic

beams transmit to the lens and focused into the particles-deionized (DI)-water suspension within the microchannel. The acoustic energy is absorbed by water and particles prior to the reflection by the silicon reflection wall, and then the beams backtrack to the transducer and are characterized.

Figure 2 shows the geometry design of the lens and ZnO transducer. ZnO thin films are easy to obtain and to integrate within the microfluidic chip by simple sputtering and lift-off processes. Particularly, the thicknesses of the ZnO film we can reach ( $\sim 4\ \mu\text{m}$ ) make it possible to work in this high frequency range. The paraxial acoustic focal length of the lens, as in the case of optical lens, the paraxial acoustic focal distance, is given by

$$f = \frac{n}{n-1}R, \quad (1)$$

where  $f$  is the focus length measured from the top of the lens,  $n$  is the relative acoustic index,  $n = \frac{v_{\text{si}}}{v_{\text{w}}} = 5.7$ ,  $v_{\text{si}} = 8432\ \text{m/s}$  is the longitudinal acoustic velocity in silicon, and  $v_{\text{w}} = 1482\ \text{m/s}$  is in water at  $20^\circ\text{C}$ .

Making use of the geometry relationship, the aperture width  $A$  can be deduced from  $A = 2R\sin\theta$ . The length of the transducer is equal to the aperture so that all of the generated acoustic beams can be focused by the lens. The length of the transducer is linked to the aperture of the lens, while the width of the transducer is linked to the depth of the microchannel. In our design, the width of the transducer is fixed to be  $120\ \mu\text{m}$  and the area  $S = 55\ 080\ \mu\text{m}^2$  has been planned in order to match the real part of electrical impedance of the

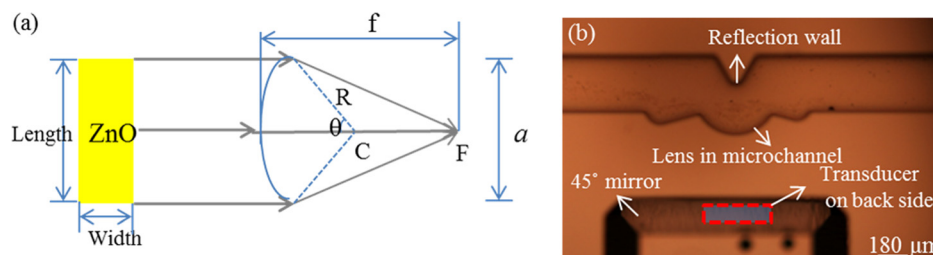


FIG. 2. Scheme of the acoustic wave transmission through an acoustic lens. (a) Structure chart of the cylindrical lens and (b) photo of the  $45^\circ$  mirror-lens system. The width of the reflection wall is  $30\ \mu\text{m}$ .  $R$  is the radius of lens,  $\theta$  is the angle of aperture,  $a$  is the aperture,  $C$  is the center of the curvature, and  $F$  is the focus. The length of the transducer is the same as that of the aperture.

TABLE I. Geometrical parameters of the cylindrical lenses and corresponding real parts of the impedance of the ZnO film transducer at 650 MHz.

Parameter	80	100	120	150
Lens radius R ( $\mu\text{m}$ )	80	100	120	150
Angle of curvature $\theta$ ( $^\circ$ )	60	60	60	60
Focal length F ( $\mu\text{m}$ )	97	121	146	182
Aperture A ( $\mu\text{m}$ )	139	173	208	260
Transducer area ( $\mu\text{m}^2$ )	16560	20760	24960	31200
Real part impedance ( $\Omega$ )	165.5	132.5	110.3	88

transducer. Setting at the resonance frequency  $f_r = 650$  MHz for the ZnO film and using the formula

$$R(f_r) = \frac{A}{Sf_r^2} - j \frac{1}{C_0} \frac{1}{2\pi f_r}, \quad (2)$$

where  $C_0$  is the static capacitance of the transducer. The real part impedance of transducer  $R(\Omega)$  for different lens can be calculated, as shown in Table I.

For acoustic excitation integrated in the microsystem, the incident acoustic wave undergoes various losses from the transducer to the liquid in the channel. These losses include acoustic diffraction along with propagation, absorption of acoustic energy by the liquid, and reflection losses on the interface of silicon/air/liquid. The propagation loss is a key parameter for the acoustic platform which can determine the useful signal to the noise ratio. The Vector Network Analyzer (VNA, Rohde&Schwarz ZVA8) was used to measure the complex response of the device in the frequency domain and provides the loss parameters.

In the case of the focalization of the acoustic beam by lens, the amplitude distribution in the focal plane can be modified with respect to the paraxial focal length. To determine the experimental focal distance of the acoustic lens, a channel is designed with the same lens geometry on one side of the channel and three different distances of a small reflector on the other side. As shown in Fig. 3, the distances of the three reflectors (L1, L2, and L3) are the expected paraxial focal length. The maximal channel width is designed from the top of the lens to the reflection wall. The radius of the lens is  $150 \mu\text{m}$  with an angle of aperture of  $60^\circ$ . Thus, the predicted focal length is  $364 \mu\text{m}$ .

KI solution is commonly used in acoustic characterization because its acoustic velocity is independent of concentration and nearly constant.<sup>20</sup> Here, 3 mol/l KI solution is injected into the lens and the  $S_{11}$  (return loss) reflection

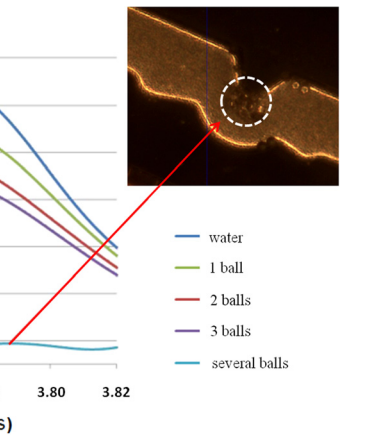
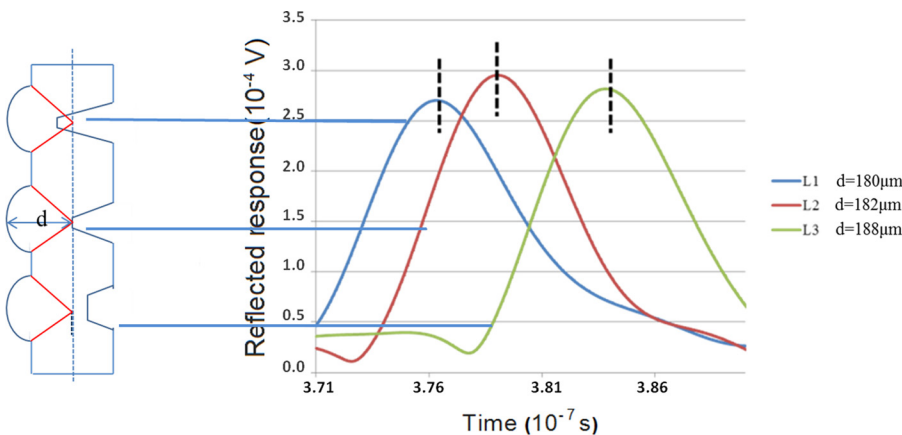


FIG. 4.  $S_{11}$  parameters for the detection of  $30 \mu\text{m}$  PS balls in lens with different numbers. The inset figure shows the ball aggregation around the reflection wall.

coefficient is measured. The acoustic beams are generated from the ZnO transducer, reflected by the  $45^\circ$  mirror, and propagate into the KI solution in the microchannel, focused by the lens into the reflection wall, and then the beams return along the original path and back to the transducer. The  $S_{11}$  parameters reflect acoustic attenuation of the propagation in this system. For channel L2,  $d$  (distance between the reflector and the bottom of lens) is  $182 \mu\text{m}$ , and the amplitude of  $2.92 \times 10^{-4} \text{V}$  is the maximal in the three channels. This distance  $d_0 = 182 \mu\text{m}$  is the predicted value for half of the paraxial focal length, and the estimated value of the depth of focus is around  $\pm 5 \mu\text{m}$ . In principle, for the channel with more deviation of the  $d_0$ , there is higher acoustic attenuation and thus the amplitude is lower. However, the figure displays that channel L1 ( $2 \mu\text{m}$  distance deviation) has the lowest amplitude of  $2.68 \times 10^{-4} \text{V}$ , while channel L3 ( $6 \mu\text{m}$  distance deviation) has a higher amplitude of  $2.80 \times 10^{-4} \text{V}$ . Then, it can be deduced that the virtual focal length is between  $182 \mu\text{m}$  and  $188 \mu\text{m}$  for the lens in this device.

$30 \mu\text{m}$  polystyrene (PS) balls are used to characterize the detection sensitivity of the lens system (radius:  $150 \mu\text{m}$  and focal length:  $182 \mu\text{m}$ ). A microfluidic pump is used to inject particles into the microchannel, and PS particles are accurately driven to the focal area of the lens. As shown in Fig. 4, the numbers of balls which remain in the lens are counted and the  $S_{11}$  reflection coefficient is measured. The amplitude of the transmitted signal on the linear scale of the

FIG. 3. Characterization of lens with different focal lengths using the  $S_{11}$  reflection coefficient in the time domain. 3 mol/l KI liquid was used and L1:  $d = 180 \mu\text{m}$ , time echo is 376 ns; L2:  $d = 182 \mu\text{m}$ , time echo is 379 ns; L3:  $d = 188 \mu\text{m}$ , time echo is 384 ns.  $d$ : distance between the reflector and the bottom of lens.

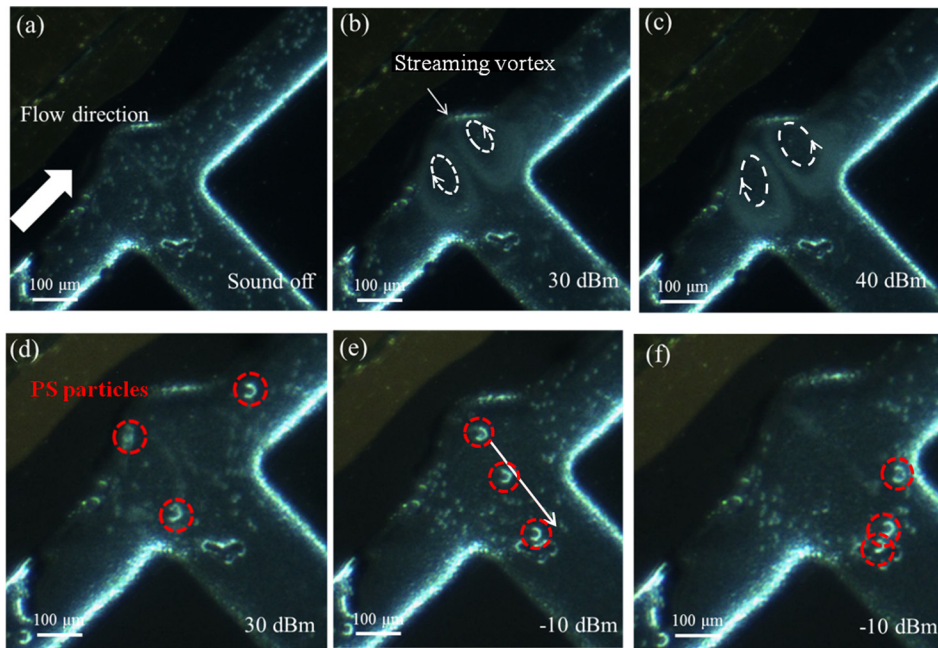


FIG. 5. Acoustic focusing in lens (radius:  $150\ \mu\text{m}$  and focus length:  $364\ \mu\text{m}$ ) for strong mixing of  $9\ \mu\text{m}$  particles (a)–(c) and separation of  $30\ \mu\text{m}$  particles (d)–(f) in the T-shape micro-channel. Red dashed lines indicate  $30\ \mu\text{m}$  particle movement.

network analyzer is normalized to 1 V of the emitted signal. For the case of pure water, the maximum amplitude of  $1.18 \times 10^{-4}\ \text{V}$  is presented which shows larger attenuation with particle balls. Through controlling the liquid flow, the number of balls one by one in the lens area is increased. The  $S_{11}$  reflection coefficient for 1 ball of PS particles is  $9.88 \times 10^{-5}\ \text{V}$  with a 16.3% deviation from water, and for 2 balls, the amplitude is decreased to  $8.69 \times 10^{-5}\ \text{V}$  with a 26.3% deviation from water. For 3 balls' detection, the signal can also be recognized with an amplitude of  $7.80 \times 10^{-5}\ \text{V}$ , with a deviation of 33.8%. The deviation accuracy (around 10%) showed the ability for the lens system to discriminate single particles in fluid. As the elastic balls gather in the detection area, the acoustic attenuation is reduced and thus the  $S_{11}$  amplitude is also decreased. On another aspect, when the balls reach a certain quantity (several balls around 10 balls), the amplitude is too low to be discriminated from the level of acoustic noise. As seen in the inset figure, ball aggregation occurred around the reflection wall; this phenomenon may be due to a diffusion process when the acoustic waves are spread and absorbed by particles.

For suspended micro-objects in the acoustic field, they are under a competitive interaction of the gravitational force, the buoyancy force, the acoustic radiation force, and the Stokes drag force induced by acoustic streaming. In our case of particle manipulation, the acoustic streaming phenomenon plays a leading role in agitation of particles in the micro-channel. The streaming phenomenon is due to the absorption of acoustic energy but independent of the particle size. Thanks to the lens design, acoustic energy can be directed to the focal region and the longitudinal vibrations attenuating on the reflection wall generate highly localized velocity as well as acceleration fields.

Here, the lens structure in a fork structure channel for strong mixing is demonstrated to separate PS particles. As shown in Figs. 5(a)–5(c),  $9\ \mu\text{m}$  PS particles in water are injected into the microchannel. When the acoustic field is excited with a 30 dBm input power, a strong streaming is

generated by highly focused acoustic energy while two vortex streamlines formed around the focus plane. Particles in the fluid in the lens area appear to rotate and align themselves along the streamlined shape. In this effect, streaming motions are presented in the particle trajectory with a spherical focusing. When the input power is increased to 40 dBm, the streaming motions are noticeably more vigorous beyond the beam, and  $9\ \mu\text{m}$  PS particles are highly stirred. To further study the acoustic streaming effect in particles,  $9\ \mu\text{m}$  PS particles and  $30\ \mu\text{m}$  PS particles were injected into the T-shape micro-channel. As shown in Figs. 5(d)–5(f), strong streamings are excited in 30 dBm input power. Both large particles ( $30\ \mu\text{m}$ ) and small particles ( $9\ \mu\text{m}$ ) are yielded to the acoustic field and move in a vortex. However, when the input power is decreased to  $-10\ \text{dBm}$ , larger particles which suffer larger added mass force start to move in a straight line to the focus point, while small particles still follow the vortex streamlines. After several seconds, the large particles reach the focus point and stay still in the balance of viscous drag force and acoustic radiation force.

In summary, a 650 MHz high frequency acoustic device functioned locally has been developed in microfluidics. The use of the confocal lens structure is validated and presents excellent performance, and single particles can be discriminated in acoustic characterization. In addition, particle manipulation depending on the size can be achieved in the same device. Future work will aim at the integration process for single cancer cell characterization and preliminary separation in microfluidic chips for *in situ* analysis.

This work was supported by the National Natural Science Foundation of China (No. 81572860), the National Key R&D Program of China (No. 2017YFF0108600), and the National Major Scientific Instruments Development Project of China (No. 81527801). The French government and University of Valenciennes for the Ph.D. grant support and also Renatech Network which partially supported this activity are acknowledged.

- <sup>1</sup>T. J. DuBose, *J. Diagnostic Med. Sonography* **1**, 205 (1985).
- <sup>2</sup>T. J. DuBose and A. L. Baker, *J. Diagnostic Med. Sonography* **25**, 173 (2009).
- <sup>3</sup>H. Lüers, K. Hillmann, J. Litniewski, and J. Bereiter-Hahn, *Cell Biophys.* **18**, 279 (1991).
- <sup>4</sup>J. Melin and S. R. Quake, *Annu Rev. Biophys. Biomol. Struct.* **36**, 213 (2007).
- <sup>5</sup>J. Xi, J. Y. Chen, M. P. Garcia, and L. S. Penn, *J. Biochips Tissue Chip* **S5**, 1–10 (2013).
- <sup>6</sup>K. Länge, B. E. Rapp, and M. Rapp, *Anal. Bioanal. Chem.* **391**, 1509 (2008).
- <sup>7</sup>R. B. Ishay, Y. K. Barnea, I. Grigoriantz, E. Teblum, and J. P. Lellouche, *Sens. Actuators, B* **215**, 373 (2015).
- <sup>8</sup>Z. Wang and J. Zhe, *Lab Chip* **11**, 1280 (2011).
- <sup>9</sup>M. Antfolk and T. Laurell, *Anal. Chim. Acta* **965**, 9 (2017).
- <sup>10</sup>A. Nilsson, F. Petersson, H. Jönsson, and T. Laurell, *Lab Chip* **4**, 131 (2004).
- <sup>11</sup>S. S. Guo, L. B. Zhao, K. Zhang, K. H. Lam, S. T. Lau, X. Z. Zhao, Y. Wang, H. L. W. Chan, Y. Chen, and D. Baigl, *Appl. Phys. Lett.* **92**, 213901 (2008).
- <sup>12</sup>S. B. Q. Tran, P. Marmottant, and P. Thibault, *Appl. Phys. Lett.* **101**, 114103 (2012).
- <sup>13</sup>F. Guo, P. Li, J. B. French, Z. Mao, H. Zhao, S. Li, N. Nama, J. R. Fick, S. J. Benkovic, and T. J. Huang, *Proc. Natl. Acad. Sci. U.S.A.* **112**, 43 (2015).
- <sup>14</sup>M. Wiklund, R. Green, and M. Ohlin, *Lab Chip* **12**, 2438 (2012).
- <sup>15</sup>D. J. Collins, Z. Ma, J. Han, and Y. Ai, *Lab Chip* **17**, 91 (2017).
- <sup>16</sup>W. Jung, J. Han, J. W. Choi, and H. A. Chong, *Microelectron. Eng.* **132**, 46 (2015).
- <sup>17</sup>S. Wang, J. Gao, J. Carlier, P. Campistron, A. NDiaguene, S. Guo, O. B. Matar, D. C. Dorothee, and B. Nongaillard, *Ultrasonics* **51**, 532 (2011).
- <sup>18</sup>S. Li, J. Carlier, F. Lefebvre, P. Campistron, D. Callens, G. Nassar, and B. Nongaillard, *Phys. Procedia* **70**, 918 (2015).
- <sup>19</sup>J. Gao, J. Carlier, S. X. Wang, P. Campistron, D. Callens, S. S. Guo, X. Z. Zhao, and B. Nongaillard, *Sens. Actuators, B* **177**, 753 (2013).
- <sup>20</sup>J. Attal and C. F. Quate, *J. Acoust. Soc. Am.* **59**, 69 (1976).